IEEE Access
Multidisciplinary | Rapid Review | Open Access Journal

Received February 1, 2018, accepted April 5, 2018, date of publication April 18, 2018, date of current version May 9, 2018.

Digital Object Identifier 10.1109/ACCESS.2018.2827704

Effect of Damper Winding and Stator Slot Skewing Structure on No-Load Voltage Waveform Distortion and Damper Bar Heat in Large Tubular Hydro Generator

ZHEN-NAN FAN[1], LI-HAN[2], YONG LIAO[2], LI-DAN XIE[3], KUN WEN[1], JUN WANG[1], XIU-CHENG DONG[1], AND BING YAO[1]

[1]Key Laboratory of Fluid and Power Machinery, Ministry of Education, Xihua University, Chengdu 610039, China
[2]State Key Laboratory of Power Transmission Equipment and System Security and New Technology, Chongqing University, Chongqing 400030, China
[3]Jiangsu Linyang Microgrid Technology Company Ltd., Nanjing 211112, China

Corresponding author: Zhen-Nan Fan (fanzhennan@126.com)

This work was supported in part by the National Natural Sciences Fund, Youth Fund of China, under Grant 51607146 and Grant 61703345, in part by the Key Scientific Research Fund Project of Xihua University under Grant Z1520907 and Grant Z1520909, in part by the Key Research Fund Projects of the Sichuan Provincial Education Department under Grant 16ZA0155 and Grant 16ZB0159, in part by the Sichuan Science and Technology Program under Grant 2018GZ0391, in part by a grant from the Chunhui Project Foundation of the Education Department of China under Grant Z2016144, and in part by the Key Laboratory of Fluid and Power Machinery, Ministry of Education, Xihua university, Chengdu, China.

ABSTRACT We study the influence of the damper bar pitch, the stator slot skewing degree, and the damper bar number per pole on the no-load voltage waveform harmonic distortion factor (HDF) and the damper winding heat of a tubular hydro generator. We implemented 288 different design schemes using a 36-MW fractional-slot tubular hydro generator. The following influence factors were investigated: continuous variation, variation range, variation step, and higher-order harmonics of no-load voltage. Thus, the relation among these structure parameters and the HDF, the losses, and the highest temperature of the damper bars is revealed. In addition, the calculated models and results are validated directly by test data, and measures are proposed for their improvement. The present research not only corrected the errors in the related papers we published before, but also provides guidelines for optimizing the no-load voltage waveform and decreases the damper bar losses and heat, as well as a more comprehensive, accurate, and effective reference for improving tubular hydro generator design and manufacture.

INDEX TERMS Waveform aanlysis, electromagnetic fields, losses, thermal analysis, hydroelectric generator.

I. INTRODUCTION

In tubular hydro generator design, the selection of damper winding and stator slot structure parameters—such as damper bar pitch, stator slot skewing degree, and damper bar number per pole—has significant influence not only on the distribution of losses and the heat of the damper winding but also on the distortion of no-load voltage waveforms. The variation tendency of the no-load voltage waveform harmonic distortion factor (HDF) and the damper bar heat with the above structure parameters are extremely important. It can not only reveal the influence of the continuous variation of these structural parameters on the no-load voltage waveform and the damper bar heat but also provide more clear guidance for improving these waveforms and reduce damper heat.

To comprehensively and accurately study these influences and their curves, the following three requirements should be considered in detail in the analysis process. First, the structure parameter variation range should be set wide enough to include the parameter values that have been calculated or recorded so far. Then, the structure parameter variation step should be set small enough to include all the meaningful parameter values. Finally, in the analysis of the HDF variation trends with the structure parameters, the effects of higher-order harmonics should be considered more fully. That is to say, not only the tooth harmonics but also other higher-order harmonics, should be considered.

Although some fruitful achievements were obtained in the calculation and analysis of the electric machinery voltage and

the rotor heat [1]–[14], only one study was conducted on the variation rule of the no-load voltage waveform HDF and the damper bar heat with the above structure parameters [14].

In [14], from eight different design schemes, the no-load voltage waveforms of a 36-MW tubular hydro generator were optimised, and the damper bar heat was reduced with the design scheme by adjusting the damper bar pitch and the stator slot skewing degree. The accuracy and rationality of its calculation models were verified via a voltage and field-winding average temperature test. However, compared with the above requirements, [14] had the following deficiencies.

First, in [14], the structure parameter variation was not wide enough. For example, the scope of t_2/t_1 was limited between 0.6 and 0.93, where t_1 was the stator slot pitch and remained stable and t_2 was the damper bar pitch and was varied. As a result, certain values were not considered, such as the values between 0.5 and 0.6 that had been adopted in some early generators and the values larger than 1 that were adopted in some generators in recent years. Furthermore, for the number of damper bars per pole n_b, [14] only discussed the structure with $n_b = 4$, and the other common structures with $n_b = 3$ and $n_b = 2$ were not considered.

Second, the structure design schemes discussed in [14] are very few (only eight schemes) and the structure parameter variation step is too wide. For example, the variation step of t_2 and the stator slot skewing degree are 0.1 t_1 and $0.25t_1$, respectively. Therefore, some meaningful parameter values may be omitted. Consequently, it is difficult to accurately and sufficiently analyse the influence of the continuous variation of these two parameters on the no-load voltage waveform HDF and the damper bar heat.

Third, in [14], although the impacts of the 1st to 50th harmonics are considered in the no-load waveform HDF calculation, only the impacts of tooth harmonics are considered in discussing the trends of HDF with the structure parameters variation; this can hardly explain the changing rule of HDF with some structure parameters, such as the stator slots skewing degree. Therefore, the comprehensiveness and accuracy of these trends analysis can still be further improved.

In addition, in [14], only the average temperature of field winding is measured, and the damper bar temperature cannot be tested directly. Thus, it is difficult to satisfactorily verify the accuracy and rationality of the calculation results of the damper winding loss and heat.

To overcome these shortcomings of [14], in the present study, the no-load voltage and the damper winding heat of 288 different design schemes of a 36-MW fractional-slot tubular hydro generator ($q = 1^1/_2$) are comprehensively and systematically analysed. The structure parameter variation range is wider and the variation step is smaller, as shown in Table 1. In addition, higher no-load voltage harmonics are considered in the HDF trends analysis. The influence of these structure parameters' continuous variation on the no-load voltage waveform HDF and the damper winding losses and heat is revealed. Furthermore, the damper bar loss and heat calculate model and results are directly verified through the damper winding temperature test. Based on these results, the no-load voltage waveform HDF and the damper winding heat are reduced more effectively by more appropriately choosing these structure parameters.

TABLE 1. The different structure design schemes.

Scheme	n_b	t_2/t_1	Stator slot skewing
1	4	0.5–0.93, $\Delta_{t2/t1} = 0.01$	0
2	3	0.5–1.32, $\Delta_{t2/t1} = 0.01$	0
3	2	0.5–1.50, $\Delta_{t2/t1} = 0.01$	0
4	4	$t_2/t_1 = 0.93$	0~1 slot, Δ_{skew} = 0.05slot
5	3	$t_2/t_1 = 0.93$	0~1 slot, $\Delta_{skew} = 0.05$ slot
6	2	$t_2/t_1 = 0.93$	0~1 slot, $\Delta_{skew} = 0.05$ slot

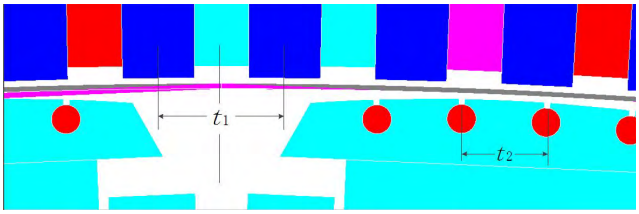

FIGURE 1. The stator slot pitch t_1 and the damper bar pitch t_2.

TABLE 2. The basic data of the generator.

Parameter	Value
Rated power (MW)	36
Rated voltage (kV)	10.5
Rated current (A)	2151
Rated power factor	0.92
Number of poles	72
Number of damper bars per pole	4
Number of stator slots per pole per phase	$1^1/_2$

In Table 1, t_1 is the stator slot pitch and remains constant, and t_2 is the damper bar pitch and can vary, as shown in Fig. 1. $\Delta_{t2/t1}$ is the change step of t_2/t_1, Δ_{skew} is the change step of the stator slot skewing degree, and n_b is the number of damper bars per pole. As the poleshoe width is invariant, the t_2/t_1 change regions for the different n_b values are different.

II. CALCULATION MODELS

A. GENERATOR PARAMETERS

The specifications of the generator in this study (SFWG36-72/7350) and the basic data of the generator are listed in Table 2.

B. MULTI-SLICE MOVING ELECTROMAGNETIC FIELD-CIRCUIT COUPLING MODEL OF THE GENERATOR

The influence of the skewed stator slot structure was analysed, with reference to the literature [15] and [16], to build up a multi-slice moving electromagnetic field-circuit coupling model of the generator.

According to the periodicity of the magnetic field of generator, a pair of poles was chosen as the electromagnetic field

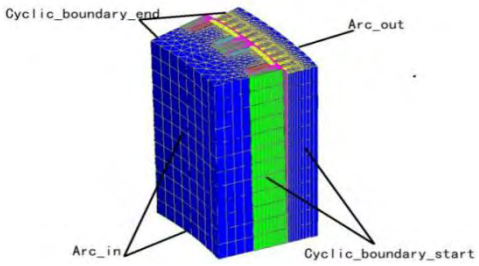

FIGURE 2. Problem regions and FE meshes of electromagnetic fields (3-D time-step FEM).

calculation region. For the stator slot skewed structural design scheme, the generator was divided into twelve equal slices along the axial direction,as shown in Fig.2.

Considering the saturation of an iron core, the 3D boundary value problem of a nonlinear time-varying electromagnetic moving field is obtained:

$$\begin{cases} \nabla \times (v\nabla \times \mathbf{A}) + \dfrac{1}{\rho}\left[\dfrac{\partial \mathbf{A}}{\partial t} - \mathbf{V} \times (\nabla \times \mathbf{A})\right] = \mathbf{J_S} \\ \mathbf{A}|_{Arc\_in} = \mathbf{A}|_{Arc\_out} = 0 \\ \mathbf{A}|_{Cyclic\_boundary\_start} = \mathbf{A}|_{Cyclic\_boundary\_end} \end{cases} \tag{1}$$

where $\mathbf{A}$ is the magnetic vector potential, $\mathbf{J_s}$ is the source current density, v is the reluctivity, $\mathbf{V}$ is the velocity and ρ is the resistivity.

For each slice, the current density and magnetic vector potential have only the axial z component, and the speed has only the circumferential x component. With the Coulomb norm $\nabla \cdot \mathbf{A} = 0$ and the boundary condition of the problem region, the 2D boundary value problem of a nonlinear time-varying moving electromagnetic field for the generator is then obtained:

$$\begin{cases} \dfrac{\partial}{\partial x}(v\dfrac{\partial A_{slz}}{\partial x}) + \dfrac{\partial}{\partial y}(v\dfrac{\partial A_{slz}}{\partial y}) = -j_{slz} + \dfrac{1}{\rho}\dfrac{\partial A_{slz}}{\partial t} \\ \qquad + \dfrac{V_x}{\rho}\dfrac{\partial A_{slz}}{\partial_x} \\ A_{slz}|_{arc\_in} = A_{slz}|_{arc\_out} = 0 \\ A_{slz}|_{cyclin\_boundary\_start} = A_{slz}|_{cyclic\_boundary\_end} \end{cases} \tag{2}$$

where V_x is the circumferential component of velocity, J_{slz} is the axial component of source current density and A_{slz} is the magnetic vector potential.

To consider the influence of the stator end winding and the rotor damper winding end rings, the coupling circuit models are established, as discussed in the literature [17]–[19]. The stator coupling circuit is shown in Fig. 3(a). The stator winding parallel branch number is one, for each slice; therefore the voltage equation of the stator circuit is

$$e_s = u_{oc} + R_{1e}i_s + L_{1e}\frac{di_s}{dt} \tag{3}$$

where e_s, u_{oc} and i_s are the inductive EMF, the voltage and the current, respectively, of the stator phase winding. R_{1e} and L_{1e} are the resistance and the leakage inductance, respectively,

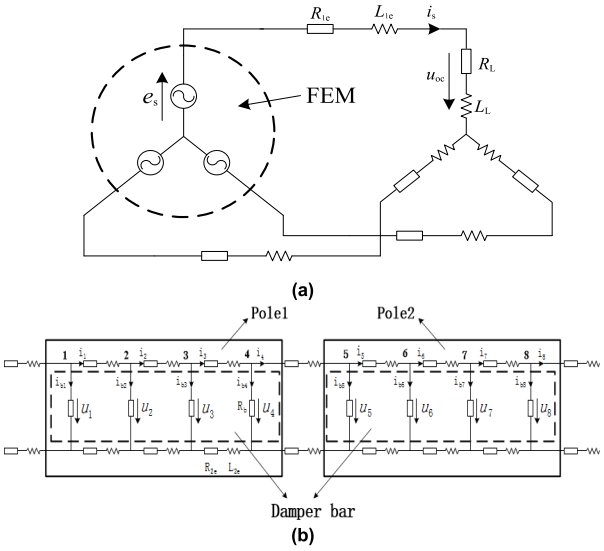

FIGURE 3. Coupling circuit. (a) Coupling circuit of the stator winding. (b) Coupling circuit of the damper winding in the problem region (with two poles and all damper bars connected in a cage).

of the stator end winding, R_L is the resistance of the load and L_L is the inductance of the loads.

In the rotor of this tubular hydro-generator, there are 4 damper bars on every pole. The problem region studied in this work contains only two poles; thus, there are 8 damper bars in total. Fig. 3(b) shows the circuit of damper bars in the problem region for every slice, as demonstrated previously in the literature [17], and all damper bars are connected in a cage.

Supposing that i_{k-1} and i_k are the end ring currents on the left and right branches of kth damper bar, respectively, the relationship between i_{k-1}, i_k and the current of the damper bar i_{bk} can be obtained:

$$i_k - i_{k-1} + i_{bk} = 0 \tag{4}$$

The voltage equation to describe the relationship between the kth and (k + 1)th branches of the damper bars is

$$u_k - u_{k+1} = 2i_kR_{2e} + 2L_{2e}\frac{di_k}{dt} \tag{5}$$

where R_{2e} and L_{2e} are the resistance and the inductance of the damper winding end ring, respectively.

From the periodic condition, the constraint conditions of the current and the voltage on the boundary are

$$i_1 + i_n + i_{b1} = 0 \tag{6}$$

$$u_n - u_1 = 2i_nR_{2e} + 2L_{2e}\frac{di_n}{dt} \tag{7}$$

where n is the number of damper bars in the problem region. When n is 8, the following equations are obtained:

$$i_1 + i_8 + i_{b1} = 0 \tag{8}$$

$$u_8 - u_1 = 2i_8R_{2e} + 2L_{2e}\frac{di_8}{dt} \tag{9}$$

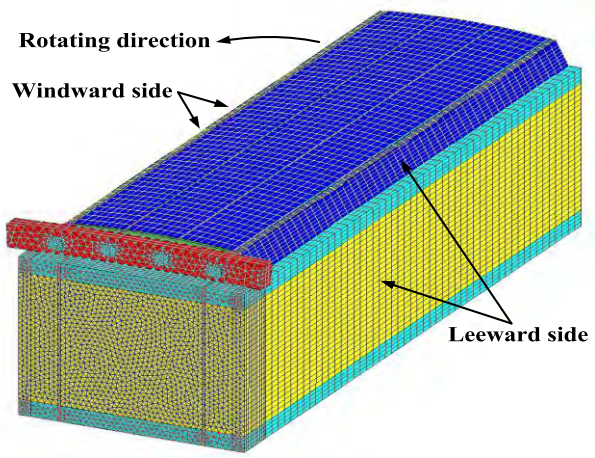

FIGURE 4. Problem region of 3D temperature field(3D steady temperature field).

If the stator and rotor coupling circuit equations and the electromagnetic field equations are combined, the magnetic vector potential A_{slz} of slices can be calculated by the time-step FE method; then, the no-load votage,and the eddy current losses of damper bars(the heat sources of damper bars) can be acquired.

C. BOUNDARY VALUE PROBLEM OF ROTOR 3D TEMPERATURE FIELD

In the rotor temperture field model construction,the following 2 key points must be considered.

Firstly,because of the existence of air gap, the influence of stator winding loss on the heat of the rotor is neglected.

Secondly,the generator use the symmetrical ventilation air cooling,and because of the symmetric structure of the rotor pole and its ventilation system,the distribution of rotor temperature field is mirror symmetric on the both sides of the rotor shaft middle profile.

Therefore, an half axial section of the rotor, which consists of rotor core, damper bar, field winding and its bracket, *et al.*, is selected as the problem region for the 3D temperature field solving, as shown in Fig.4.

Considering the anisotropic heat conduction condition of rotor core, the boundary value problem of 3D steady temperature field can be expressed as follows:

$$\begin{cases} \dfrac{\partial}{\partial x}(\lambda_x \dfrac{\partial T}{\partial x}) + \dfrac{\partial}{\partial y}(\lambda_y \dfrac{\partial T}{\partial y}) + \dfrac{\partial}{\partial z}(\lambda_z \dfrac{\partial T}{\partial z}) = -q_V \\ \lambda \dfrac{\partial T}{\partial n}\Big|_{S_A} = 0 \\ \lambda \dfrac{\partial T}{\partial n}\Big|_{S_B} = -\alpha(T - T_f) \end{cases} \tag{10}$$

where T is the temperature, λ_x, λ_y, λ_z are the heat conductivity on each direction respectively, q_v is the heat source density which is obtained by the loss calculation mentioned above, S_A is the rotor middle profile and the interface between rotor core and rim related with the thermal insulation boundary condition, S_B is the outside surface of the rotor related with the heat dissipation boundary condition, α is the heat dissipation coefficient of S_B, and T_f is the environment air temperature.

According to Hydro-generator typical design manual, The heat dissipation coefficients on the end and top surfaces of the pole shoe and field winding are as following respectively [1]:

$$\alpha = \frac{1 + 0.1\tau}{450} \tag{11}$$

$$\alpha'' = K\alpha' \tag{12}$$

where τ is the pole pitch, $K$and α' are the coefficients related with the generator structure respectively.

Considering the better cooling condition on the windward, the heat dissipation coefficients of the pole shoe and field winding are enlarged by certain proportion respectively. On the other hand, the heat dissipation coefficients on the lee side of the pole shoe and field winding are reduced by certain proportion respectively due to their worse cooling condition.

III. COMPUTATION RESULTS AND DISCUSSION

A. THE NO-LOAD VOLTAGE WAVEFORM QUALITY

In the no-load voltage analysis, HDF is used to define the deviation between the actual and the sinusoidal waveforms of the line voltage according to the Chinese National Standard GB/T 1029-2005 [20]:

$$HDF = \frac{\sqrt{U_2^2 + U_3^2 + \cdots\cdots + U_n^2}}{U_1} \times 100\% \tag{13}$$

where $U_k(k = 1, 2, 3, \ldots n$; n is the highest order considered) is the line voltage value of the k^{th} harmonic.

For large generators, HDF must not exceed 5% [20].

Some results are presented on Fig.5, and some phenomena can be obtained as follows.

① By adjusting only the damper bar pitch t_2 and keeping the stator slot unskewed, when $t_2/t_1 \in$ [0.5,0.6], or $t_2/t_1 \in$ [0.9,1.0], or $t_2/t_1 > 1.3$ with $n_b = 2$, HDF is large, and the no-load voltage waveform quality is bad. When $t_2/t_1 \in$ [0.75,0.9], or $t_2/t_1 \in$ [1.2,1.3] with $n_b = 3$ or 2, a smaller HDF and a better no-load voltage waveform are obtained.

② Different skew of the stator slots can lead to different HDF reductions. For example, schemes with a stator slot skewing of 0.25 t_1, 0.55 t_1, or 0.8 t_1 cannot reduce HDF effectively, so the waveforms are not good enough. On the other hand, with schemes with a stator slot skew of 0.4 t_1, 0.45 t_1, 0.5 t_1, 0.6 t_1, 0.9 t_1, or t_1, the optimised waveform can be achieved, and the best waveform is obtained with the stator slot skewing of t_1. Comparison of these stator slot skewed schemes, which have smaller HDF and better waveforms, indicates that HDF differences are not obvious. Especially, the HDF values for the stator slot skew of 0.45 t_1 and t_1 are almost the same, as shown in Table 3. This means that with the smaller stator slot skew-degree schemes, such as 0.45 t_1, almost optimum no-load waveforms can still be obtained.

③ Comparison of the schemes in which the t_2/t_1 value is adjusted without the stator slot skew (Fig. 5(a)) shows

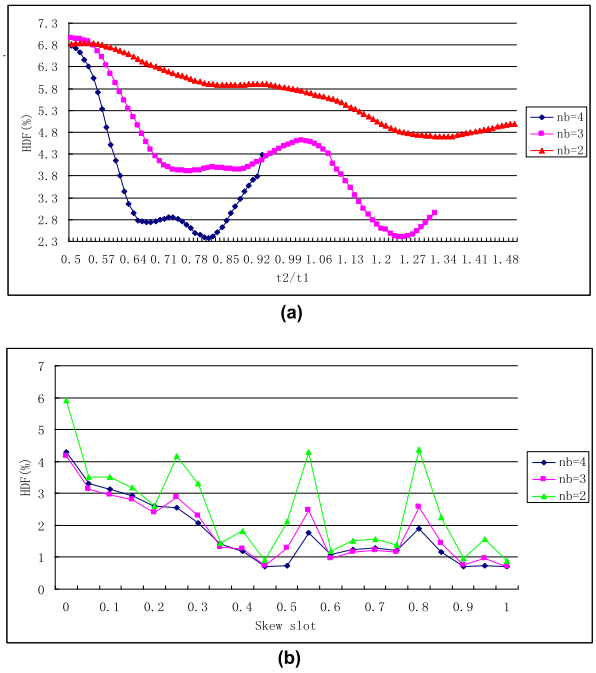

FIGURE 5. The curve of HDF. (a) The curve of HDF with different t_2/t_1 (stator slot no-skewed). (b) The curve of HDF with different stator slot skewing degree ($t_2/t_1 = 0.93$).

TABLE 3. The different skew degrees investigated in this study.

Skew degree	$n_b = 4$	$n_b = 3$	$n_b = 2$
0.40 t_1	1.185%	1.271%	1.816%
0.45 t_1	0.711%	0.730%	0.899%
0.50 t_1	0.752%	1.283%	2.121%
0.60 t_1	1.081%	0.955%	1.178%
0.90 t_1	0.742%	0.747%	0.959%
1.00 t_1	0.709%	0.728%	0.897%

that, for a large number of damper bars per pole n_b, HDF may be reduced more effectively and a better waveform will be obtained. For the stator slot skewed schemes (Fig. 5(b)), the curve shapes are similar, but HDF can be reduced more effectively when n_b is larger.

Compared with [14], the following obviously improvements are achieved by the above results.

As the t_2/t_1 variation range (0.5 to 1.42) is much wider than that of [14] (0.6 to 0.93), $t_2/t_1 > 1$ schemes may still possible to get lower HDF. This result can explain why $t_2/t_1 > 1$ was adopted in some empirical design schemes in recent years. On the contrary, the result obtained in [14] cannot be attributed to the t_2/t_1 variation range if $t_2/t_1 > 1$ was not included.

Increasing the damper bar number per pole reasonably can reduce HDF effectively. This result can explain why the schemes with $n_b = 4$ or 3 and $q = 1^1/_2$ were recommended by some early classic design manuals. On the contrary, such results could not be obtained in [14] because it only considered the scheme with $n_b = 4$.

As the stator slot skew degree variation step in the present study (0.05 t_1) is much smaller than that of [14] (0.25 t_1), the obtained series of skewing degrees can produce lower or higher HDF values. This result not only indicates that increasing the skew degree cannot guarantee HDF reduction, but also provides more comprehensive and accurate references for better skew degree selection.

In addition, compared with the no-skewed scheme, the stator slots skewed scheme requires higher welded machining accuracy of the stator core key bars. That means more sophisticated techniques, more working hours, and higher labour cost. Furthermore, the stator slot skewed scheme increases the length of the stator bar (strands). Therefore, it requires more material and is more expensive. Therefore, the manufacturing cost of the stator slot skewed scheme is higher than that of the no-skewed scheme. Thus, increasing the skewing degree increases the manufacturing cost. Here, we propose a series of skewing degrees, in which the HDF values approximates that of the best waveform scheme (skew degree is t_1), leading to manufacturing cost reduction.

Based on the above results, relative to [14] which discusses only eight design schemes, we describe the relationship between the HDF and the structure parameters more comprehensively, accurately, and reasonably, while also suggesting more accurate range and value for these structure parameters to restrain HDF.

Furthermore, to explain the above results, we perform harmonic analysis of the no-load voltage waveforms, including higher-order harmonics.

The ordinal number of tooth harmonics is:

$$\nu = \beta 2mq \pm 1 \tag{14}$$

where β is the order of the tooth harmonic, m is the number of phases, and q is the number of stator slots per pole per phase. Here, the ordinal number of the 1st order and the 2nd order tooth harmonics is 8th and 10th, and 17thand 19th, respectively.

To observe the extreme values of the harmonic components of the no-load voltage waveform, the distribution of the no-load voltage harmonics of some design schemes is shown as Fig. 6. To show the harmonics distribution more clearly, the fundamental wave component is not shown in these figures, which should be 100%.

The no-load voltage spectrum diagrams of Fig. 6 indicate that the 27th and 29th harmonics are significant besides the tooth harmonics. Therefore, in addition to the tooth harmonics, the 27th and 29th harmonics should also be considered carefully.

The change of the above voltage harmonics with t_2/t_1 and the stator slots skew degree are shown in Figs. 7–9.

In particular, with respect to the change of t_2/t_1 and the stator skew degree, the influence of the 1st order tooth harmonics can be neglected. However, the influence of the 2nd order tooth harmonics and the higher-order harmonics (the 27th and the 29th) are obvious.

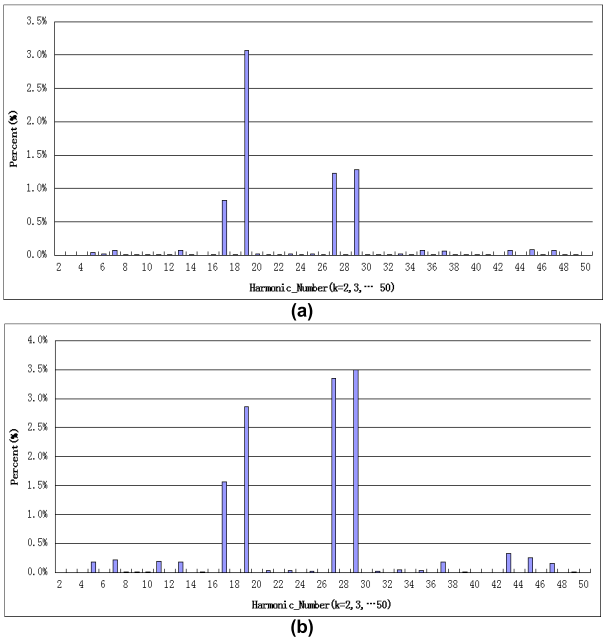

FIGURE 6. The voltage harmonics distribution at no-load. (a) $n_b = 4$, $t_2/t_1 = 0.93$ and no stator slot skewed. (b) $n_b = 2$, $t_2/t_1 = 0.93$ and no stator slot skewed.

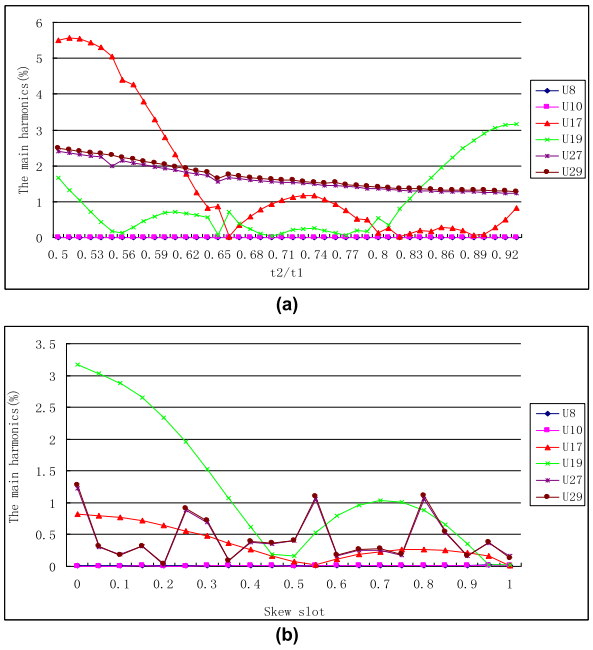

FIGURE 7. The main voltage harmonics variation at no-load with $n_b = 4$. (a) Change t_2/t_1, no stator slot skewed. (b) Change stator slot skew degree, $t_2/t_1 = 0.93$.

To analyse the influence of the 2nd order tooth harmonics and the higher harmonics (the 27th and the 29th) on HDF, the parameterF_u is then defined as follows:

$$F_u = \sqrt{\frac{U_{17}^2 + U_{19}^2 + U_{27}^2 + U_{29}^2}{U_1}} \times 100\% \qquad (15)$$

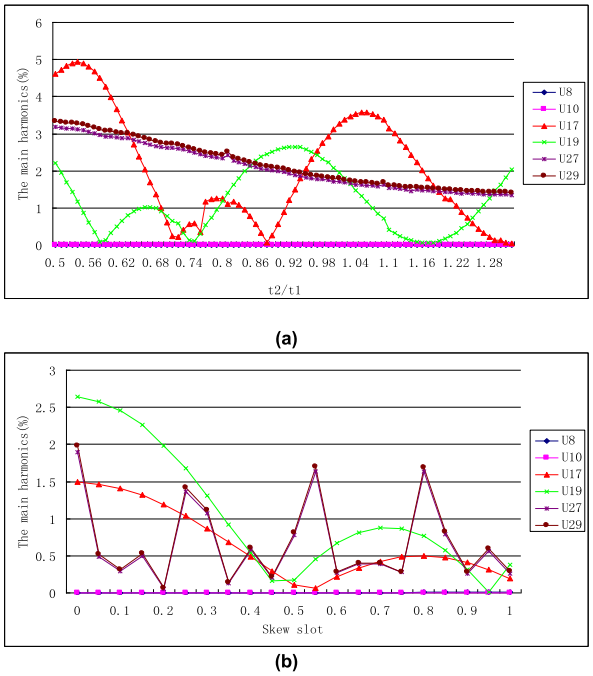

FIGURE 8. The main voltage harmonics variation at no-load with $n_b = 3$. (a) Change t_2/t_1, no stator slot skewed. (b) Change stator slot skew degree, $t_2/t_1 = 0.93$.

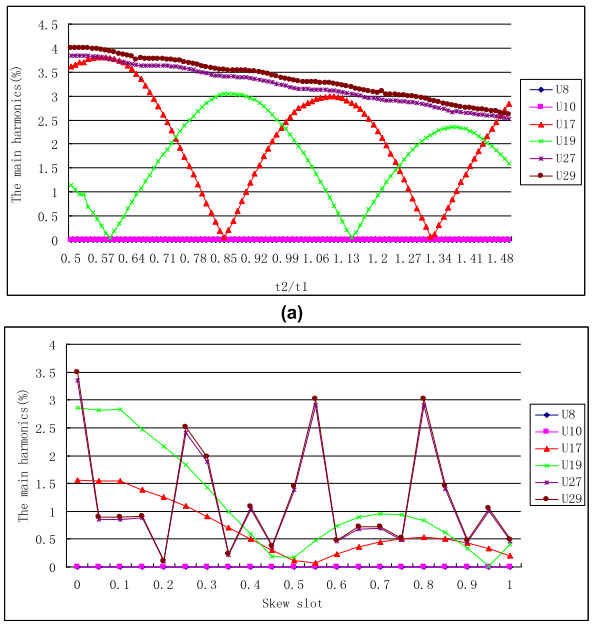

FIGURE 9. The main voltage harmonics variation at no-load with $n_b = 2$. (a) Change t_2/t_1, no stator slot skewed. (b) Change stator slot skew degree, $t_2/t_1 = 0.93$.

The change of F_u with t_2/t_1 and the stator skew degree is shown as Fig.10.

By Figs. 7−10, some phenomena can be seen as follows.

① The F_u-t_2/t_1 curves and the degree of the stator slot skewing are almost the same with those of Fig. 5, where HDF changes with these two parameters. These results indicate that for the tubular hydro generator with the $q = 1^1/_2$, besides the

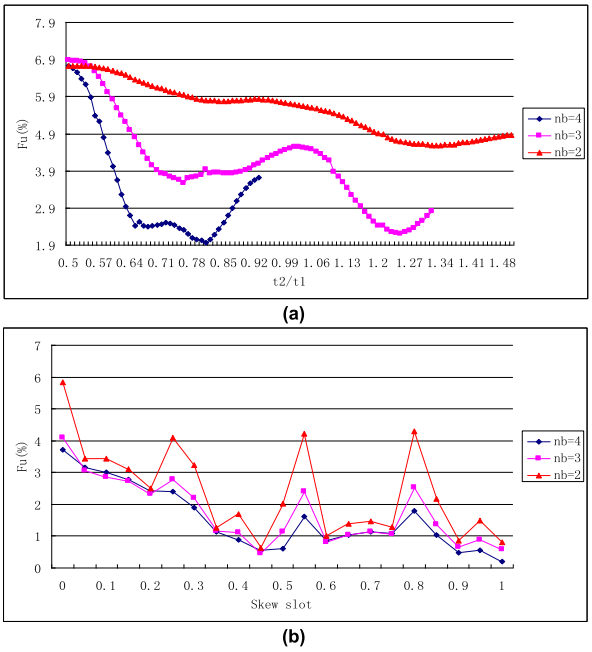

FIGURE 10. The influence of main voltage harmonics on HDF of no-load voltage. (a) change t_2/t_1, no stator slot skewed. (b)$t_2/t_1 = 0.93$, change the skew degree of stator slot.

2nd order tooth harmonics (17th and 19th), the 27th and 29th harmonics have a decisive influence on the no-load voltage HDF value.

② Only increasing the t_2/t_1 value without the stator slot skew, the 27th and the 29th harmonics continue to decline. But this measure cannot ensure the reduction of the 2nd order tooth harmonics (17th and 19th) effectively, especially when $t_2/t_1 \in [0.5, 0.6]$ or $t_2/t_1 \in [0.9, 1.0]$, or $t_2/t_1 > 1.3$ with $n_b = 2$. The 2nd order tooth harmonics are very obvious, so the HDF is large and the no-load voltage waveform quality is bad. In the regions where the 2nd order tooth harmonics and the 27th and 29th harmonics have smaller values at the same time, a smaller HDF and a better no-load voltage waveform can be obtained, as in the case when $t_2/t_1 \in [0.75, 0.9]$ or $t_2/t_1 \in [1.2, 1.3]$ with $n_b = 3, 2$.

③ Skewing the stator slots can reduce the 2nd order tooth harmonics (17th and 19th) effectively, but some skewing stator slots schemes may produce larger 27th and 29th harmonics, and then increase HDF and reduce the waveform quality, such as in the schemes with 0.25 t_1, 0.55 t_1, and 0.8 t_1 are skewed. For some other schemes, which have smaller 2nd order tooth harmonics and the 27th and 29th harmonics at the same time, a smaller HDF and a better waveform can be obtained, such as in the case when 0.4 t_1,0.45 t_1, 0.5 t_1, 0.6 t_1, 0.9 t_1, and t_1 are skewed.

Compared with [14], the following obvious improvements can be obtained.

As the no-load voltage waveform HDF of this generator is not only affected by the 2nd order tooth harmonics (17th and 19th), but also by the 27th and the 29th higher harmonics, only considering the tooth harmonics cannot guarantee accuracy and rationality of the HDF trends analysis. In particular, in the analysis of the stator slot skewing schemes, if only the tooth harmonics are considered, as in [14], the variation tendency of the HDF change with the stator slot skewing degree cannot be explained.

In this paper, we consider also the higher harmonics, and thus the HDF trends analysis becomes more accurate and efficient. In particular, the influence of the 27th and the 29th harmonics is considered, and the variation tendency of HDF with the stator slot skewing degree is explained well.

According to the above results, in comparison with the [14], the present study that considers the impacts of other high harmonics could give a more accurate and reasonable explanation for the HDF pattern with changing structure parameters.

TABLE 4. The T_{max} of different skew degree $t_2/t_1 = 0.93$.

Skew degree	$n_b = 4$	$n_b = 3$	$n_b = 2$
0.40 t_1	146.05℃	136.61℃	115.59℃
0.45 t_1	145.81℃	136.48℃	115.49℃
0.50 t_1	145.43℃	135.76℃	115.48℃
0.60 t_1	145.36℃	136.09℃	115.41℃
0.90 t_1	144.94℃	135.84℃	115.40℃
1.00 t_1	144.85℃	135.50℃	115.39℃

B. THE LOSSES AND HEAT OF DAMPER BARS

When the generator operates at a rated load, the losses and the heat of damper bars are shown as Fig. 11 and Table 4.

In these figures, $\sum p$ represents the losses at the entire damper bars in a rotor pole,T_{max} represents the maximum temperature of these damper bars.

Compared with [14], the following improvements can be proposed based on the above results.

Increasing only t_2/t_1 cannot guarantee the reduction of the damper bar losses and heat. In addition, combined with the no-load voltage analysis results of this paper, we can find that although some empirical design schemes with $t_2/t_1 > 1$ are possible to obtain lower HDF, the damper bar heat may be higher. On the contrary, because the $t_2/t_1 > 1$ schemes are not considered in [14], the continuous increase of t_2/t_1 was considered sufficient to reduce the damper bar losses and the heat.

Furthermore, based on the present no-load voltage analysis results, although decreasing the damper bar number per pole can reduce the damper bar losses and heat, this measure will worsen the no-load voltage waveform. These results indicate that some $n_b = 2$ schemes, which were adopted in some recent generators, may be inappropriate. On the contrary, this result could not be obtained in [14] because it only considered the scheme with $n_b = 4$.

In addition, the above results indicate that, compared with [14], more design schemes that restrain the HDF and the damper bar heat at the same time are obtained.

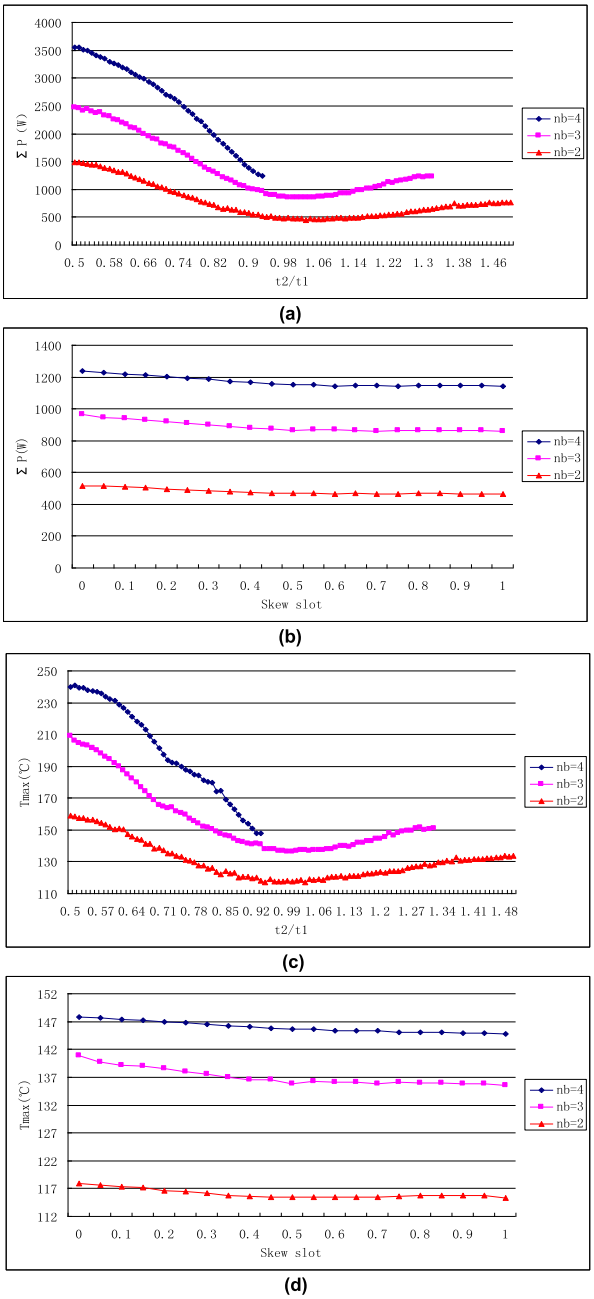

FIGURE 11. The losses and the temperature of damper bar. (a) The losses of damper bars at rated-load with no stator slot skewed. (b) The losses of damper bars at rated-load with $t_2/t_1 = 0.93$ and tator slot skewed. (c) The T_{max} of damper bars at rated-load with no stator slot skewed. (d) The T_{max} of damper bars at rated-load with $t_2/t_1 = 0.93$ and stator slot skewed.

C. VERIFICATION OF THE NO-LOAD VOLTAGE CALCULATION

The test wiring diagram is shown in Fig. 12(a). The basic data of the potential transformer in the test are listed in Table 5, and the no-load voltage test and calculation values are compared in Fig. 12(b) and 12(c).

The comparison of the above calculation and the measured values of the harmonics with the HDF shows that the results are similar. This proves that the model presented here has high accuracy in analysing the quality of the no-load voltage waveform.

TABLE 5. Potential transformer data.

Parameter of potential transformer	Value
Rated voltage U_N (kV)	10.5
Accuracy classification	0.2
Voltage error (%)	±0.2
Phase error (')	±10
Frequency rating (Hz)	50

TABLE 6. The generator operation condition in the test.

Parameter	Value	Parameter	Value
Active power (MW)	320	Rated power factor	0.9
Stator voltage (kV)	17.4	Field voltage (V)	264
Stator current (kA)	10.7	Field current (A)	1527

TABLE 7. The equipment in FIGURE 13.(b).

Position	Equipment	Position	Equipment
1	Static receiving component	5	Special wire clip
2	Microcomputer temperature measuring instrument	6	The upper end shaft
3	Rotating transmitting component	7	The lead of temperature test components
4	Special wire clip and copper pipe		

D. VERIFICATION OF THE LOSS AND HEAT CALCULATION

As the generator used here is operating at a hydropower station, the station does not allow us to test the damper winding temperature directly. Consequently, to verify the loss and heat calculation model, we test the damper winding temperature of a vertical hydro generator in another station that allows temperature measurements, and we calculate its damper winding loss and temperature using the present calculation model.

The generator operation conditions in the test are shown in the Table 6.

The temperature test is conducted using the MF51 semiconductor thermistors, which are solid-pasted on the test points, as shown as Fig. 13(a). In Fig. 13(b), the equipment in positions 1–7 is listed in Table 7. In addition, a block diagram of the temperature test system is shown in Fig. 13(c). In this test system, infrared coding technology is adopted for the signal transmission between the rotor and stator.

To shield against electromagnetic interference and protect the temperature test components, copper pipes are installed in some locations, such as rotor brackets on the surface and inside the upper shaft.

Some test results are compared with the calculated results in Table 8.

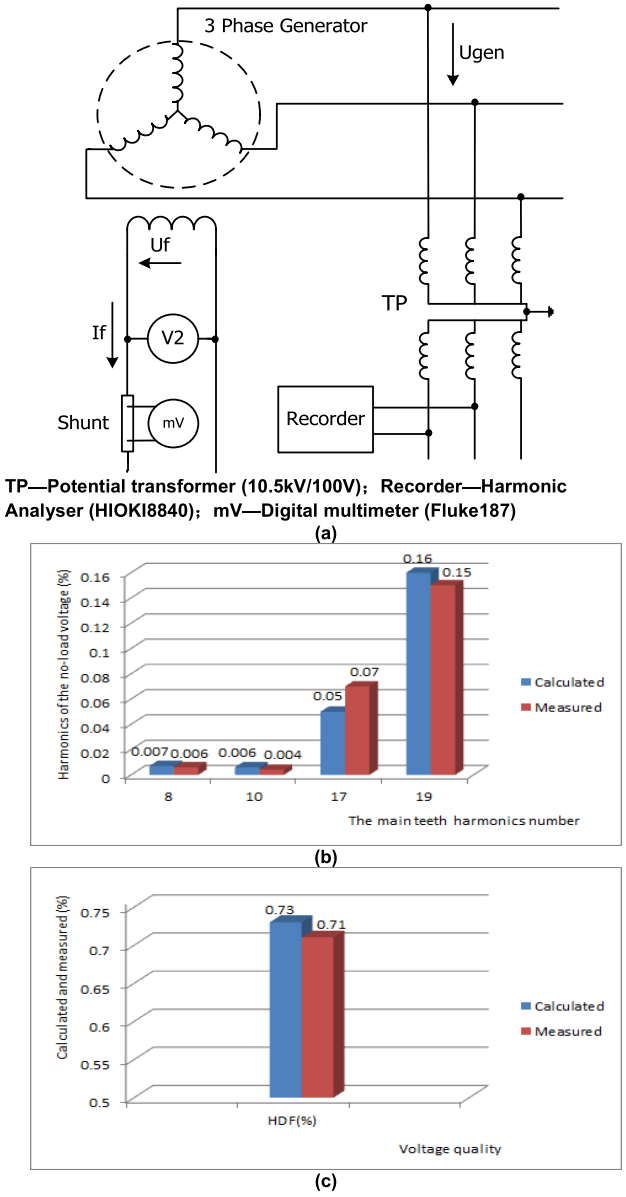

FIGURE 12. No-load voltage waveform test data. (a) Wiring diagram of the voltage waveform test. (b) Calculated and measured values of harmonics. (c) Calculated and measured values of HDF and THF.

TABLE 8. The verification of damper winding temperature calculation.

Value	The test points				
	21#	23#	28#	29#	30#
Calculation value (℃)	29	31	42	44	47
Measured value (℃)	33	34	46	47	49
Error	−12.%	−8.8%	−8.7%	−6.4%	−4%

The comparison of the above calculation and the measured values of the temperature of test points shows that the results are similar.

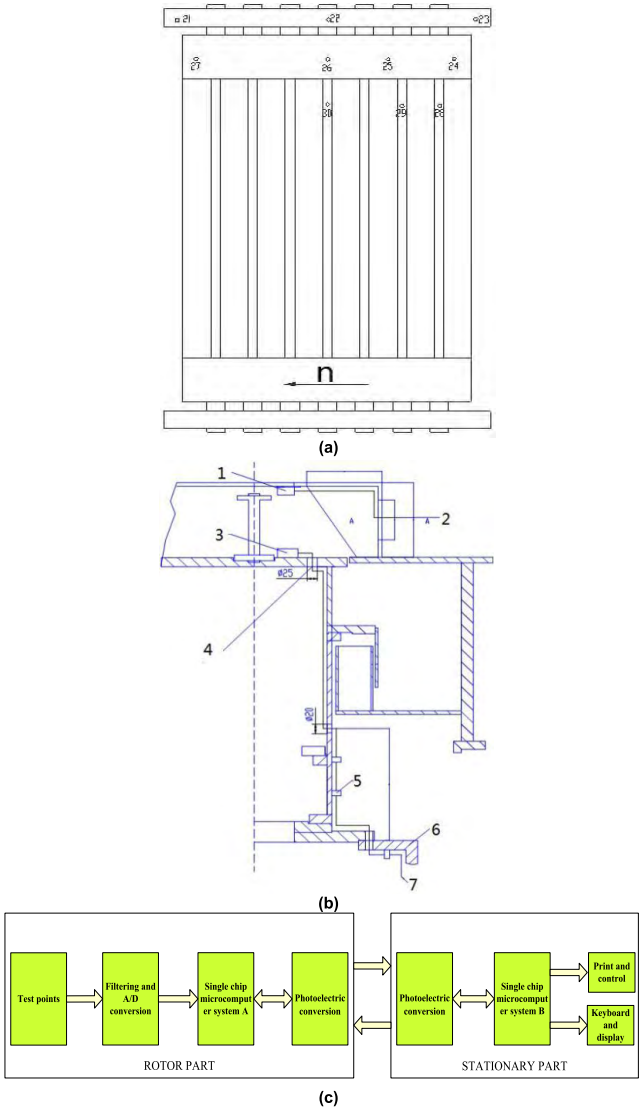

FIGURE 13. The direct temperature test of damper winding. (a) The temperature test points of damper winding. (b)The temperature test lead path. (c) The principle block diagram of temperature test system.

At the same time, it is worth noting that,it can be very difficult to measure the damper winding temperature directly for a number of reasons. First, the measure sensors are difficult to install in damper bars. Second, the power supply of the measuring instrument is difficult. Third, because the strong magnetic field in the generator,especially in the air gap,it may cause great interference to the signal transmission,so it is difficult to ensure the integrity and accuracy of the transmission of the direct sample and measure data signals of the temperature test.Fourth, the test costs are high. Especially for the tubular hydro-generator which internal space is relatively small, the damper wind temperature measurement is more difficult [21], [22].

Because of the above reasons, as of now, the China generator manufacturing enterprises and power plants rarely carry out the direct measurement of damper winding temperature, especially for the tubular hydro-generator,the direct

temperature test of the damper winding has hardly been carried out.

Therefore,up to now,the above measure values is our only on-site direct test data of damper winding temperature in hydro-generator.Although the measured generator is not the tubular hydro-generator which we are concerned,but the accuracy and rationality of our model can still be verified partly.

IV. CONCLUSION

In this paper, the defects of the [14] could be overcome well, and more comprehensive, accurate, and reasonable conclusions could be obtained as follow:

First, only simply increasing the degree of stator skewed, can not guarantee the suppression of no-load voltage waveform distortion (HDF). Some of the skewed schemes may also deteriorate the no-load voltage waveform, such as stator chute 0.25 t_1, 0.55 t_1, or 0.8 t_1, which is not considered by [14].

Second,only simply increase the damper winding pitch t_2, can not guarantee the suppress effect of damper bar loss and heat, especially the schemes of $t_2 / t_1 > 1$, there may lead to damper bar loss and heat increases.

Third, increasing the number of damper bars per pole will help suppress the HDF of the no-load voltage waveform, but at the same time, it will lead to an increase of loss and heat of the damping bars.

Fourth, when analyzing the influence trends of structural parameters on the no-load voltage waveform quality, we should not only consider the influence of tooth harmonics, but also include the influence of other higher harmonics. For example,in this paper, due to the influence of 27th and 29th harmonics were considered, we can calculate,analyze and explain the influence trend of stator slot skewed degree on HDF more accurately.

Based on this, the paper reveals and analyzes the influence trends of some structural parameters on the no-load voltage HDF and damper bar loss and heat of a 36 MW ($q = 1^1/_2$) tubular hydro-generator more comprehensively and accurately,such as the damper bar pitch, the number of damping bars per pole and the degree of stator skewed .Which provide more comprehensive, accurate and reasonable choice of structural parameters in the design and manufacture of more effective suppression of HDF and damper bar loss and heat.

In the future research work, we intend to analyze the influence trends of the above structural parameters on HDF and damper loss and heat under the different numbers of slots per pole per phase ($q = 2, 2^1/_2, 3$) . And providing a more comprehensive, accurate and reasonable reference to further enhance the design and manufacture of such generator.

Furthermore, in our opinion, by applying some optimisation algorithms, such as the particle swarm algorithm or the simulated annealing algorithm, the research of this paper can be carried out as an important electromagnetic field and temperature field inverse problem. We plan to use another special paper to study this problem in detail in the future.

REFERENCES

[1] X.-F. Chen, *Electromagnetic Calculation of Hydro-Generator*. Beijing, China: China Water Power Press, 2011.
[2] Z. Li, "Measurement of improving no-load voltage waveforms of salient-pole synchronous generator," *J. Harbin Inst. Elect. Technol.*, vol. 6, no. 3, pp. 1–16, 1983.
[3] L. Shao, W. Hua, and M. Cheng, "Design of a twelve-phase flux-switching permanent magnet machine for wind power generation," in *Proc. 17th Int. Conf. Elect. Mach. Syst. (ICEMS)*, 2014, pp. 435–441.
[4] W. Ting-Ting, L. Mei-Ling, Z. Xiao-Zhong, W. Hui-Zhen, and M. Xiao-Li, "Magnetic field analysis and structure optimization of high speed EEFS machine," in *Proc. 39th Ann. Conf. IEEE Ind. Electron. Soc. (IECON)*, Nov. 2014, pp. 978–983.
[5] J. Qudsia, I. Junaid, and B.-I. Kwon, "Analytical analysis of the magnetic field and no-load voltage for the double sided axial flux permanent magnet synchronous generator," in *Proc. 14th Biennial IEEE Conf. Electromagn. Field Comput. (CEFC)*, May 2010, p. 1.
[6] P. Bastawade, M. M. Reza, A. Pramanik, and B. N. Chaudhari, "No-load magnetic field analysis of double stator double Rotor radial flux permanent magnet generator for low power wind turbines," in *Proc. IEEE Int. Conf. Power Electron., Drives Energy Syst. (PEDES)*, Dec. 2012, pp. 1–6.
[7] M. Ranlöf, R. Perers, and U. Lundin, "On permeance modeling of large hydrogenerators with application to voltage harmonics prediction," *IEEE Trans. Energy Convers.*, vol. 25, no. 4, pp. 1179–1186, Dec. 2010.
[8] C. Bruzzese and G. Joksimovic, "Harmonic signatures of static eccentricities in the stator voltages and in the rotor current of no-load salient-pole synchronous generators," *IEEE Trans. Ind. Electron.*, vol. 58, no. 5, pp. 1606–1624, May 2011.
[9] D.-W. Zhang, Y.-J. Peng, and Z.-N. Fan, "No-load voltage waveform optimization and rotor heat reduction of tubular hydro-generator," in *Proc. 6th Int. Conf. Electromagn. Field Problems Appl. (ICEF)*, Jun. 2012, pp. 1–4.
[10] G.-H. Zhou, L. Han, Z.-N. Fan, X.-Q. Hou, and Y.-G. Liao, "No-load voltage waveform optimization of hydro-generator with asymmetric poles," *Can. Soc. Ecol. Evol.*, vol. 29, no. 15, pp. 66–73, 2009.
[11] G. Traxler-Samek, T. Lugand, and A. Schwery, "Additional losses in the damper winding of large hydrogenerators at open-circuit and load conditions," *IEEE Trans. Ind. Electron.*, vol. 57, no. 1, pp. 154–160, Jan. 2010.
[12] L. Weili, Z. Yu, and C. Yuhong, "Calculation and analysis of heat transfer coefficients and temperature fields of air-cooled large hydro-generator rotor excitation windings," *IEEE Trans. Energy Convers.*, vol. 26, no. 3, pp. 946–952, Sep. 2011.
[13] L. Weili, Z. Yu, and C. Yuhong, "Influence of rotation on rotor fluid and temperature distribution in a large air-cooled hydrogenerator," *IEEE Trans. Energy Convers.*, vol. 28, no. 1, pp. 117–124, Mar. 2013.
[14] Z.-N. Fan, Y. Liao, L. Han, and L.-D. Xie, "No-load voltage waveform optimization and damper bars heat reduction of tubular hydro-generator by different degree of adjusting damper bar pitch and skewing stator slot," *IEEE Trans. Energy Convers.*, vol. 28, no. 3, pp. 461–469, 2013.
[15] B. Weilharter, O. Biro, S. Rainer, and A. Stermecki, "Computation of rotating force waves in skewed induction machines using multi-slice models," *IEEE Trans. Magn.*, vol. 47, no. 5, pp. 1046–1049, May 2011.
[16] J. Keränen, P. Ponomarev, J. Pippuri, P. Råback, M. Lyly, and J. Westerlund, "Parallel performance of multi-slice finite-element modeling of skewed electrical machines," *IEEE Trans. Magn.*, vol. 53, no. 6, Jun. 2017, Art. no. 7201204.
[17] A. M. Knight, S. Troitskaia, N. Stranges, and A. Merkhouf, "Analysis of large synchronous machines with axial skew, part 2: Inter-bar resistance, skew and losses," *IET Electric Power Appl.*, vol. 3, no. 5, pp. 398–406, Sep. 2009.
[18] Y. Huangfu, S. Wang, J. Qiu, H. Zhang, G. Wang, and J. Zhu, "Transient performance analysis of induction motor using field-circuit coupled finite-element method," *IEEE Trans. Magn.*, vol. 50, no. 2, pp. 2283–2286, Feb. 2014.
[19] A. Sarikhani, A. Nejadpak, and O. A. Mohammed, "Coupled field-circuit estimation of operational inductance in PM synchronous machines by a real-time physics-based inductance observer," *IEEE Trans. Magn.*, vol. 49, no. 5, p. 228, May 2013.
[20] L. Fu, *The Test Measures of Three Phases Synchronous Machine*. Beijing, China: Standards Press China, 2012.

[21] M. Bergeron *et al.*, "Hydro generator damper bar current measurement at Wanapum dam," *IEEE Trans. Energy Convers.*, vol. 31, no. 4, pp. 1510–1520, Apr. 2016.
[22] H. Karmaker and A. M. Knight, "Investigation and simulation of fields in large salient-pole synchronous machines with skewed stator slots," *IEEE Trans. Energy Convers.*, vol. 20, no. 3, pp. 604–610, Sep. 2005.

ZHEN-NAN FAN was born in Longchang, China, in 1981. He received the Ph.D. degree in electrical engineering from Chongqing University, Chongqing, China, in 2013. He is currently an Associate Professor with Xihua University. His research interests include the magnetic and thermal field calculation of generators, electrical machinery, and motor drives.

LI-HAN received the M.Sc. and Ph.D. degrees in electrical machine from Chongqing University, Chongqing, China, in 1986 and 2008, respectively. He is currently a Professor with Chongqing University. His research interests include field calculation, and the design and control of electric machines.

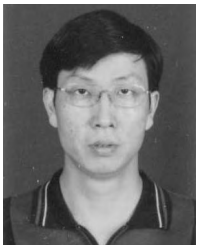

YONG LIAO received the M.Sc. degree in electrical machinery and the Ph.D. degree in power system control from Chongqing University, Chongqing, China, in 1988 and 1997, respectively. From 2001 to 2002, he was a Visiting Professor with Norhtumbria University, U.K. He is currently a Professor of electrical machinery and apparatus with Chongqing University. His research interests include the magnetic and thermal field calculation of generators and the control of doubly fed electrical machines as used in renewable energy systems. In 1998, he participated in the Global Development Program of Rockwell Automation, Milwaukee, WI, USA.

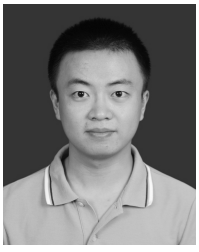

LI-DAN XIE received the M.Sc. degree in electrical engineering from Chongqing University, Chongqing, China, in 2010. He is currently an Engineer with Jiangsu Linyang Microgrid Technology Company Ltd., China. His research interests include the field calculation of generators and renewable energy.

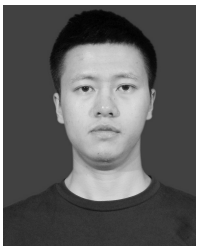

KUN WEN was born in Chongqing, China, in 1991. He is currently pursuing the M.Sc. degree with Xihua University. His research interests include the magnetic and thermal field calculation of generators, electrical machinery, and motor drives.

JUN WANG was born in Mianyang, China, in 1966. She received the Ph.D. degree in electrical engineering from Southwest Jiaotong University, Chengdu, China, in 2006. She is currently a Professor with Xihua University. Her research interests include the magnetic and thermal field calculation of generators, electrical machinery, and motor drives.

XIU-CHENG DONG was born in Xianyang, China, in 1963. He is currently a Professor with Xihua University. His research interests include the control and analysis of generators, electrical machinery, and motor drives.

BING YAO was born in Sichuan, China, in 1981. He received the M.Sc. degree from Xihua University, Chengdu, China, in 2010. He is currently a Lecturer with Xihua University. His research interests include the magnetic and thermal field calculation of generators, electrical machinery, and motor drives.